A generic coordination assembly-enabled nanocoating of individual tumor cells for personalized immunotherapy

Xiaoli Wang,‡[a] Zuoguan Chen,‡[b] Chao Zhang,[a] Chuangnian Zhang,[a] Guilei Ma,[a] Jing Yang,[a] Xiaoqing Wei,*[c] Hongfan Sun[a]*

Dr. X. Wang, C. Zhang, Dr. C. Zhang, Prof. G. Ma, Prof. J. Yang, Prof. H. Sun
Tianjin Key Laboratory of Biomaterial Research, Institute of Biomedical Engineering, Chinese Academy of Medical Sciences & Peking Union Medical College, Tianjin 300192, China. * Corresponding Author, E-mail: bmemgl@126.com

Dr. Z. Chen
Department of Vascular Surgery, Beijing Hospital, National Center of Gerontology, Chinese Academy of Medical Science & Peking Union Medical College, Beijing, 100730, China

Prof. X. Wei
Oral Biomedical Sciences, School of Dentistry, Cardiff Institute of Tissue Engineering & Repair, College of Biomedical and Life Sciences, Cardiff University, UK. * Corresponding Author, E-mail: weix1@cardiff.ac.uk

‡ Xiaoli Wang and Zuoguan Chen contributed equally to this work.

Keywords: Cell encapsulation, microparticles vaccine, tumor immunotherapy, metal–organic coordination, murine melanoma

A generic and effective tumor cells encapsulation strategy enabled by metal–organic coordination is developed to prepare vaccine for personalized immunotherapy. Specifically, epigallocatechin-3-gallate (EGCG)-Al(III) coordination layer is *in situ* formed onto individual living cell in aqueous phase, and the process can be completed within an hour. 98% of proteins in cells are entrapped within the microparticles, which endow with high antigens loading capacity. The microparticles enhance the uptake efficiency of antigens, protecte antigens from degradation in vivo, and delay the retention time of antigens in lymph node. Moreover, dendritic cells (DCs) activation is triggered by the microparticles, simultaneously, the expression of co-stimulation marker on DCs and the production of Th1-related cytokines are significantly up-regulated. Moreover, six kinds of tumor cells are utilized and successfully coated by EGCG/Al(III) layer, suggesting the generalization of this strategy. More importantly, the microparticles exhibit the comparative antitumor effect with polyinosinic-polycytidylic acid

(PolyI:C) in B16 pulmonary metastasis model. Overall, the encapsulation strategy enabled by metal–organic coordination could be potentially useful for personalized immunotherapy customized to individual patient's tumor cell.

1. Introduction

Immunotherapy that regulates the body's immune system to resist diseases, is one of the most promising therapeutic strategies for metastatic cancer.[1] The main types of immunotherapy include tumor vaccines, cell transfer therapy (DCs, NK, and T cells), and immune checkpoint blockades (CTLA-4, PD-1 and PD-L1).[2] Of which, tumor vaccines consist of defined antigens, aiming to treat and prevent tumor occurrence or recurrence after surgery. However, the development of tumor vaccines remains a challenge due to the lack of antigen, the low uptake efficiency and poor immunogenicity of antigen.[3]

Whole tumor cell lysates offer a rich source of antigens and can serve as multivalent vaccines against tumor.[4] There are four main ways to prepare tumor lysates: freeze-thaw cycles, UVB irradiation/irradiation, hypochlorous acid-oxidation, and hyperthermia.[5] Before the formation of tumor lysates, tumor cell can be modified genetically to secrete pro-inflammatory cytokines, inhibit immunosuppressive cytokines or overexpression of calreticulin.[6] To further improve the efficiency, tumor lysates can be used in association with adjuvants (IL-2) or immunomodulator (CpG, MPLA and PolyI:C),[7] or to pulse DCs for ex vivo DC-based therapy.[8] Recently, biodegradable particles (50 nm~10 μm) have been engineered to effectively deliver tumor lysates and activate DCs, including $CaCO_3$ microparticles,[9] chitosan nanoparticles,[10] yeast cell wall particles,[11] and PLGA particles.[12] Moreover, tumor lysates-derived membrane proteins were engineered into nanoliposomes,[13] PLGA nanoparticles.[14] David Mooney and colleagues co-encapsulated tumor lysates, GM-CSF and CpG into injectable cryogel for DCs recruitment and immunotherapy.[15] Besides, irradiated tumor cells coated with immunosuppressive blocker/immunocytokine were prepared as whole tumor cells vaccines.[16] Various strategies have been exploited to make whole tumor cell vaccines, for

example, tumor vaccine was obtained after knockdown the inhibitor of differentiation protein 2 in whole tumor cells.[17] However, the direct encapsulation of individual living tumor cells as tumor vaccines is rarely reported. Except in one report[18] using LbL assembly of poly(N-vinylpyrrolidone) and tannic acid onto the surface of tumor cells, yet DCs activation and the in vivo efficacy of the vaccine was not tested.

Epigallocatechin-3-gallate (EGCG), the major polyphenol in green tea, has demonstrated beneficial functions including anti-cancer, anti-HIV, anti-inflammatory effects, etc.[19] EGCG can modulate macrophages functions by upregulating Th1 cytokines (IL-12, TNF-α and INF-γ), and downregulating immunotolerance-related cytokines (IL-10).[20] Furthermore, EGCG can recover T cell suppression via inhibiting the IDO expression on tumor-associated antigen presentation cells (APCs).[21] Therefore, the use of EGCG as a vaccine component may be able to break the tolerance of tumor immunotherapy. Al(III) is the main component of aluminum adjuvant, which is the most commonly used adjuvant in humans with the capacity to provoke a strong humoral immunity. It was reported that EGCG can coordinate with Al(III) to form soluble EGCG-Al(III) complexes.[22] Moreover, Caruso and colleagues found that the coordination of tannic acid and Fe(III) can be deposited onto particle templates (such as SiO_2, $CaCO_3$ and PS spheres),[23] and yeast cells.[24] Inspired by these previous studies, we speculate that the coordination layer of EGCG-Al(III) can be formed onto the tumor cells, which provided a novel strategy for whole tumor cell vaccines that integrate immunostimulatory agents in well-defined nanocoatings of single tumor cells.

In this study, a generic strategy to prepare tumor microparticle vaccines were developed by nanocoating of individual living tumor cells with EGCG/Al(III) coordination layer. In our previous work,[25] the strategy to encapsulate individual B16 tumor cells was verified; meanwhile, the uptake of microparticles vaccine by DCs, and their therapeutic effect in B16 subcutaneous tumor model were also investigated. This work focused on the universality of this strategy to other tumor cells and the interaction between the microparticles vaccine and antigen

presentation cells (APCs) including their cytotoxicity to DCs and RAWs, and DCs activation and maturation. Furthermore, *in vivo* trafficking of the microparticles vaccines and the anti-metastatic effect of this microparticles vaccine in B16 pulmonary metastases model were also investigated. This strategy could retain almost all of the antigens and avoid time-consuming and costly antigen epitope identification. Five kinds of mouse tumor cells and one kind of human tumor cells were utilized to prove the universality of this strategy. The coordination assembly-enabled tumor cells encapsulation strategy has the clinical potential of personalized immunotherapy.

2. Results and Discussions

2.1. Encapsulation of tumor cells and preparation of TCL@EGCG/Al

A generic approach to coat individual living tumor cells with EGCG/Al coordination layers has been developed for the construction of tumor microparticles vaccine. The vaccine could be potentially useful for personalized immunotherapy customized to individual patient's tumor cells. **Figure 1a** illustrated the preparation approach. Tumor cells were coated with EGCG/Al layers by suspending in EGCG and $AlCl_3 \cdot 6H_2O$ aqueous solutions for 60 s. The process was repeated three times, leading to the formation of EGCG/Al_3 shell, respectively. After inactivation of the cells upon hypotonic treatment, the microparticles vaccine contained tumor cell lysate (TCL@EGCG/Al) were obtained.

The surface of the microparticles was rough and the size appeared homogeneous with an average diameter of 7 μm, smaller than that of live B16 cells due to the evaporation of water (Figure 1b). In comparison with TCL@EGCG/Al, uncoated B16 cells had a smoother surface. TEM images of ultrathin sections were further used to investigate the internal structure of TCL@EGCG/Al microparticles. As depicted in Figure 1c, a continuous layer encompassed the cell membrane, cytoplasm and cell nucleus, confirming the successful encapsulation of individual tumor cells with EGCG/Al layer. Besides, abnormal cell structures together with

degeneration of the cytoplasm and the cell nucleus were observed in TCL@EGCG/Al, suggesting the inactivation of tumor cells and excluding the oncogenicity of the microparticles vaccines.

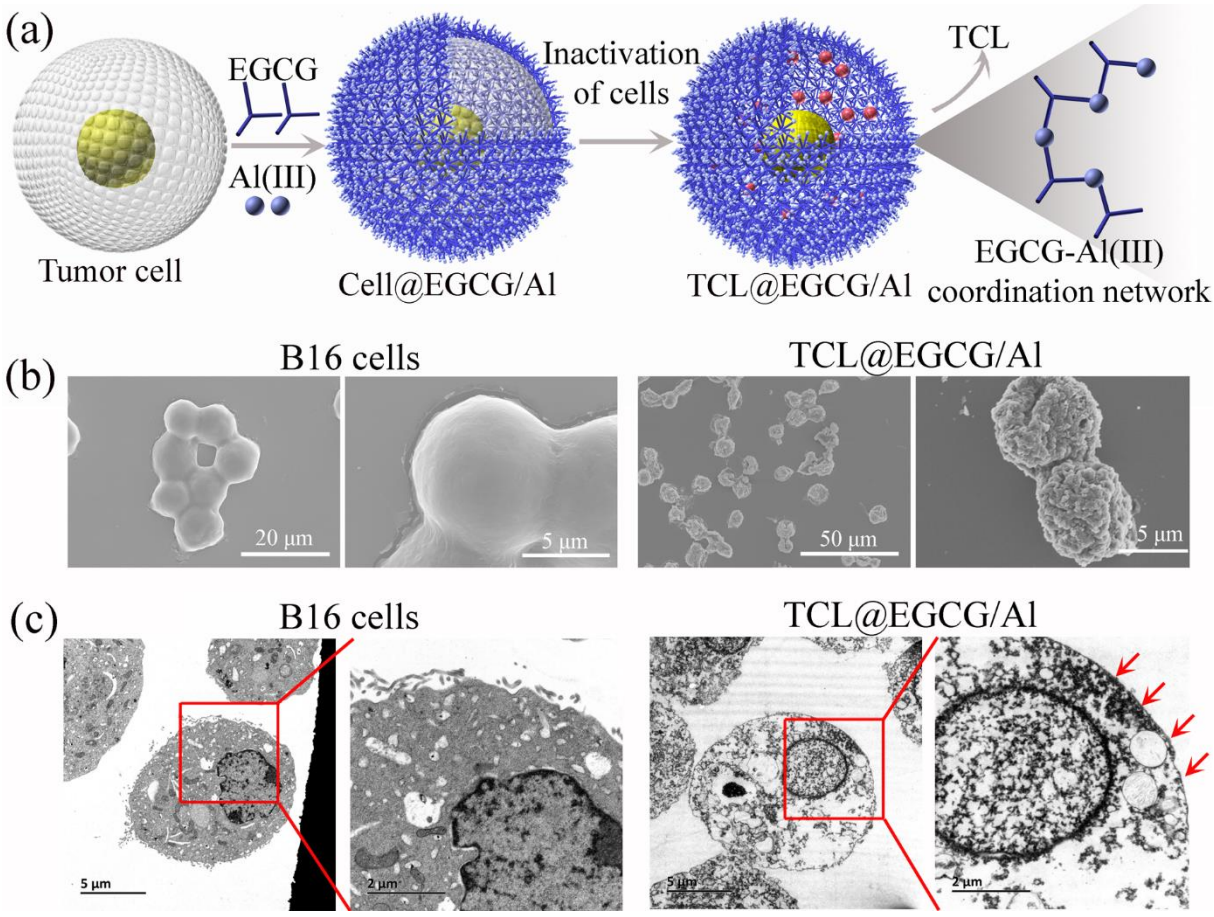

Figure 1. (a) Preparation of TCL@EGCG/Al microparticles vaccine, SEM (b) and TEM (c) images of B16 cells and TCL@EGCG/Al. The red rectangles showed a zoomed area, and the red arrows indicated the EGCG/Al coordination layer.

From CLSM images (**Figure 2a**), significantly different morphology of TCL@EGCG/Al was observed in comparison with live B16 cells, further suggesting the successful coating of cell. Besides, the size of TCL@EGCG/Al was ~13 μm, which was comparable with the size of B16 cells. Besides, dsDNA stained by DAPI was observed, indicating that the preparation process had little effect on the structure of genomic DNA. Moreover, X-ray photoelectron spectroscopy (XPS) spectrum of TCL@EGCG/Al indicated the presence of C, N, O, P, S and Al elements (Figure 2b). N, P, S and some C, O elements originated from the cells. Al and some

C, O elements came from the EGCG/Al layer. In contrast, Al element was not observed in uncoated B16 cells, indicating the formation of EGCG-Al coordination layer onto cells surface.

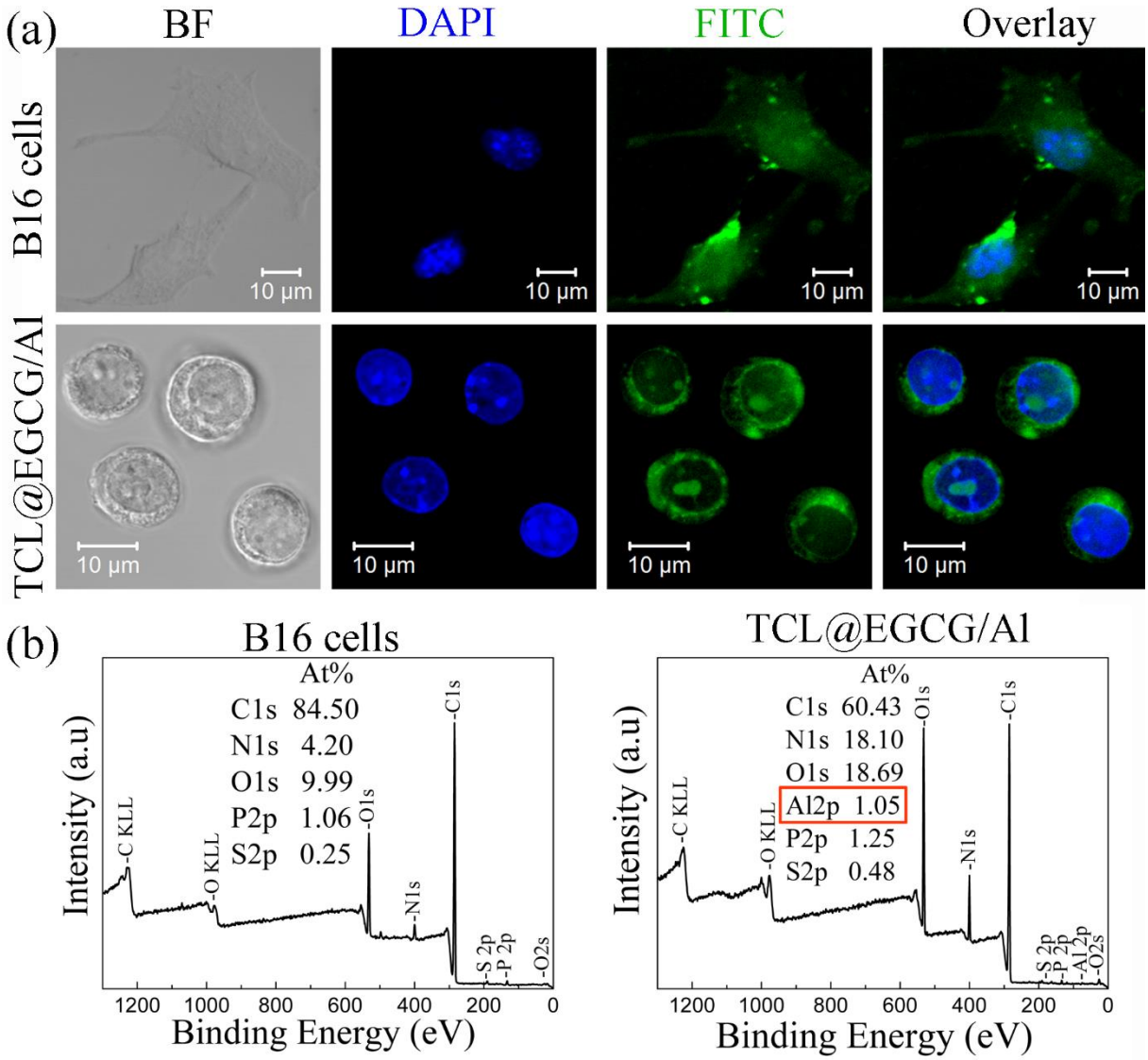

Figure 2. CLSM images (a) and XPS spectrum (b) of B16 cells and TCL@EGCG/Al.

The EGCG-Al(III) coordination layers formed rapidly independent of the nature of substrate, suggesting that the approach can be extended to other cell types. B16 cells were replaced by mouse MB49, CT26 and 4T1 cells line, and human HL-60 cells line. CLSM images showed that the distinct changes in cell morphology and intracellular structure after coating tumor cells (**Figure 3**). SEM images (**Figure S3**) showed that the size of microparticles was consistent with the cell size, but had a quite different surface topography with these templated cells. Compared to uncoated cells, the coated cells had a rougher surface. CLSM and SEM images illustrated

that the microparticles were successfully prepared with the four types of tumor cells using the identical procedure. These results demonstrate the universality of this method, which could be applied to prepare other cells-related formulations.

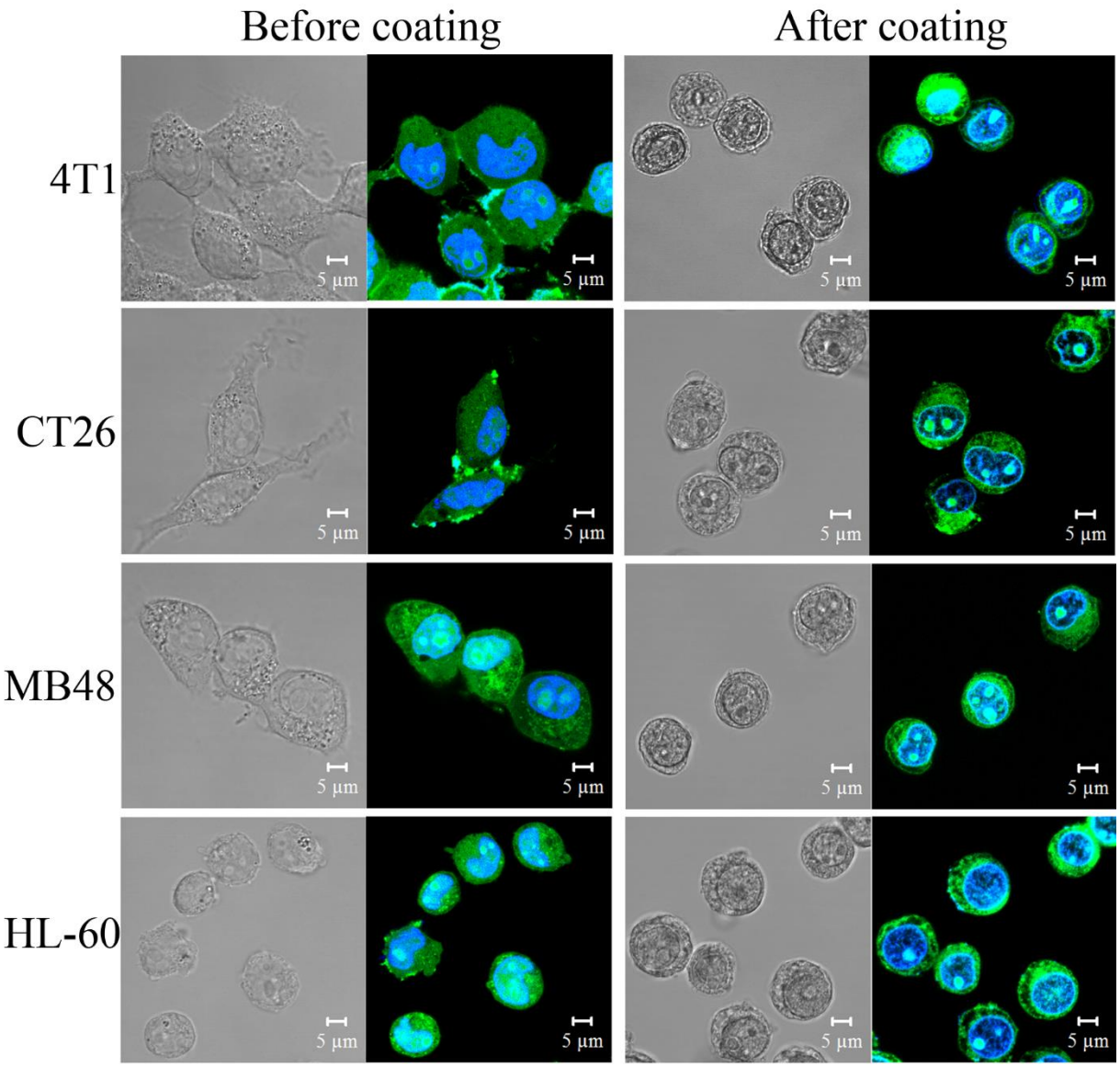

Figure 3. CLSM images of 4T1, CT26, MB49 and HL-60 cells before and after coating.

During the process, cells were repeatedly incubated in EGCG and $AlCl_3$ aqueous solution followed by centrifuging/washing. CCK-8 assay was used to investigate the effect of these mechanical procedure on cell viability, PBS control underwent the same mechanical procedure as TCL@EGCG/Al with addition of EGCG and $AlCl_3$ solution. As displayed in **Figure 4a**, the coating of EGCG/Al layer displayed significant influence on cell viability regardless of B16,

MB48 or HL-60 cells, suggesting that the effect of EGCG/Al coating on cell viability were the same. As for PBS control, the cell viabilities of B16 and HL-60 cells were not affected by these mechanical procedures; while these mechanical procedures displayed significant influence on cell viability of MB48. To ensure safe use and avoid the oncogenicity, the coated cells were further exposed to hypotonic medium by incubating them with high-purity deionized water. Upon exposure to hypotonic medium, cellular proteins might diffuse through the EGCG/Al layer, leading to the loss of tumor antigen. Measured by BCA assay, the protein amount of B16 cells was 1004.7±14.9 pg/cell. The protein amount and loading capacity of TCL@EGCG/Al prepared from B16 cells were 984.5±4.9 pg/microparticle and 497.7±2.5 ug mg^{-1} vaccine, respectively. Abount 98% of proteins in tumor cells was entrapped within TCL@EGCG/Al, avoiding the loss of tumor antigens. The protein loading capacity is higher than those of other vaccine delivery carriers such as PLGA NPs,[26] polyelectrolyte coated AuNPs,[27] and mesoporous silica NPs.[28]

The protein release rate of microparticles was pH-dependent (Figure 4b). TCL@EGCG/Al prepared from B16 cells exhibited fast protein release at pH 5.5, with 60-70% of protein released within the initial 24 h. At pH 7.4, only 30-40% of the total protein was released within 24 h. This can be ascribed to that the formation of coordination bonds between EGCG and Al^{III} is pH dependent.[29] The pH-dependent protein release was attributed to the decreased stability of EGCG-Al(III) complexes with decreasing pH.[30] The difference in stability at extracellular physiological pH (7.4) and intracellular endo/lysosome pH (5.5) was favorable for the enhanced intracellular release of protein antigens. TCL@EGCG/Al prepared from MB48 or HL-60 cells exhibited similar protein release profile with that prepared from B16 cells.

DCs, the most potent APCs, are necessary for inducing protective immunity, and macrophages are another key type of APCs. Therefore, the biocompatibility of TCL@EGCG/Al prepared from B16 cells and their respective individual constituents on DC2.4 and RAW264.7 cells were assessed (Figure 4c-d). Although EGCG exhibited distinct

cytotoxicity to DC2.4 and RAW246.7 cells at test concentrations of 100 μg/ml due to its strong reducibility. TCL@EGCG/Al and $AlCl_3$ had no distinct cytotoxicity at concentrations below 100 μg mL^{-1}, with more than 80% of cell viability after incubation with DC2.4 and RAW246.7 cells for 48 h. In addition, TCL@EGCG/Al prepared from HL-60 or MB48 cells has relatively negligible cytotoxicity to DC2.4 and RAW246.7 cells, with more than 100% of cell viability after incubation for 48 h (Figure 4e). Consequently, the cytotoxicity of the microparticles vaccine prepared from different tumor cells on APCs can be negligible.

Furthermore, the stability of TCL@EGCG/Al was also evaluated by suspending the microparticles vaccine in culture medium containing a known concentration of BSA or FBS and incubated at 37 °C. As shown in Figure 4f, the concentration of BSA in the suspension retained almost constant over the period of incubation, suggesting that the microparticles vaccine had a high stability in 1 mg mL^{-1} of BSA solution. Then, a higher protein concentration of FBS (10 v/v%, 4.46 mg mL^{-1}) was used to incubate with the microparticles vaccine. Only about 10% of FBS was adsorbed on the microparticles vaccine over the period of incubation (Figure 4f). These results revealed that the microparticles vaccine was not prone to fouling by proteins in the extracellular environment. Besides, optical images were taken after incubation for different time (**Figure S4**). Monodisperse microparticles vaccine was observed. Neither aggregation of microparticles or protein-aggregated microparticles was formed.

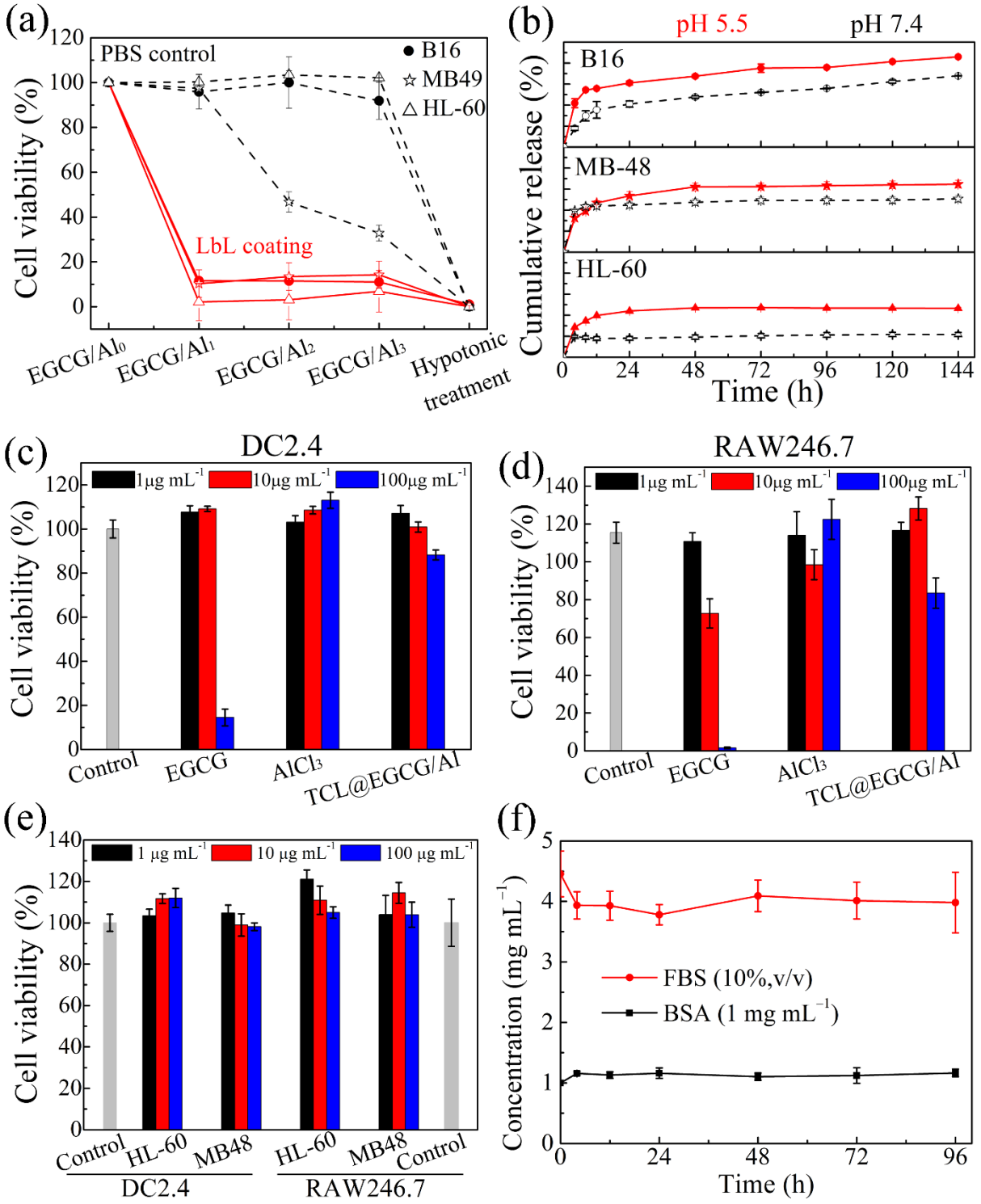

Figure 4. (a) Cell viability of B16, MB48 and HL-60 cells after each deposition cycle during preparation of TCL@EGCG/Al, the data represent mean ± SD (n = 3) (b) Time-dependent release of proteins from TCL@EGCG/Al prepared with B16, MB48 and HL-60 cells at pH 5.5 and 7.4, Cell viability of DC2.4 (c) and RAW246.7 (d) cells after incubating with TCL@EGCG/Al prepared with B16 cells and the respective materials for 48 h, (e) Cell viability

of DC2.4 and RAW246.7 after incubating with TCL@EGCG/Al prepared with MB48 and HL-60 for 48 h, culture medium was used as control, the data represent mean ± SD (n = 6), (f) The concentration of BSA and FBS as a function of time, the initial concentration of BSA and FBS (10%, v/v) was 1 mg mL^{-1} and 4.46 mg mL^{-1}, respectively, the data represent mean ± SD (n = 3).

2.2. Antigens uptake and BMDCs activation *in vitro*

BMDCs were pulsed with TCL-FITC@EGCG/Al and then observed by CLSM. From CLSM images (**Figure 5a**), the entire microparticles could be phagocytized by BMDCs although their size was quite larger. After endocytosis of the microparticles, BMDCs have prominent dendritic structures from the Z-stack CLSM image, suggesting their maturation. Live cell imaging systems were used to further reveal the endocytosis of microparticles vaccine. Considering that BMDCs is a mixed population of macrophages and DCs, its purity is based on the expression levels of CD11c. Accordingly DC2.4 is more appropriate for real-time observation of the microparticles endocytosis by live cell imaging systems, because it provided more pure population of DCs. The result demonstrated that the antigens entrapped in the microparticles vaccine can also be phagocytized by DC2.4 cells (Figure 5b and Supporting Information Video S2). It can be seen that both the entire microparticles and their debris can be phagocytized by DCs. Furthermore, FACS was further used to quantify antigen uptake (Figure 5c). About 2.5-fold increase of positive cells and 3-fold increase of the mean fluorescence intensity (MFI) were observed after co-culturing with TCL-FITC@EGCG/Al as compared to soluble TCL-FITC. This result suggested that the microparticles can significantly increase antigen uptake by DCs compared to soluble antigens.

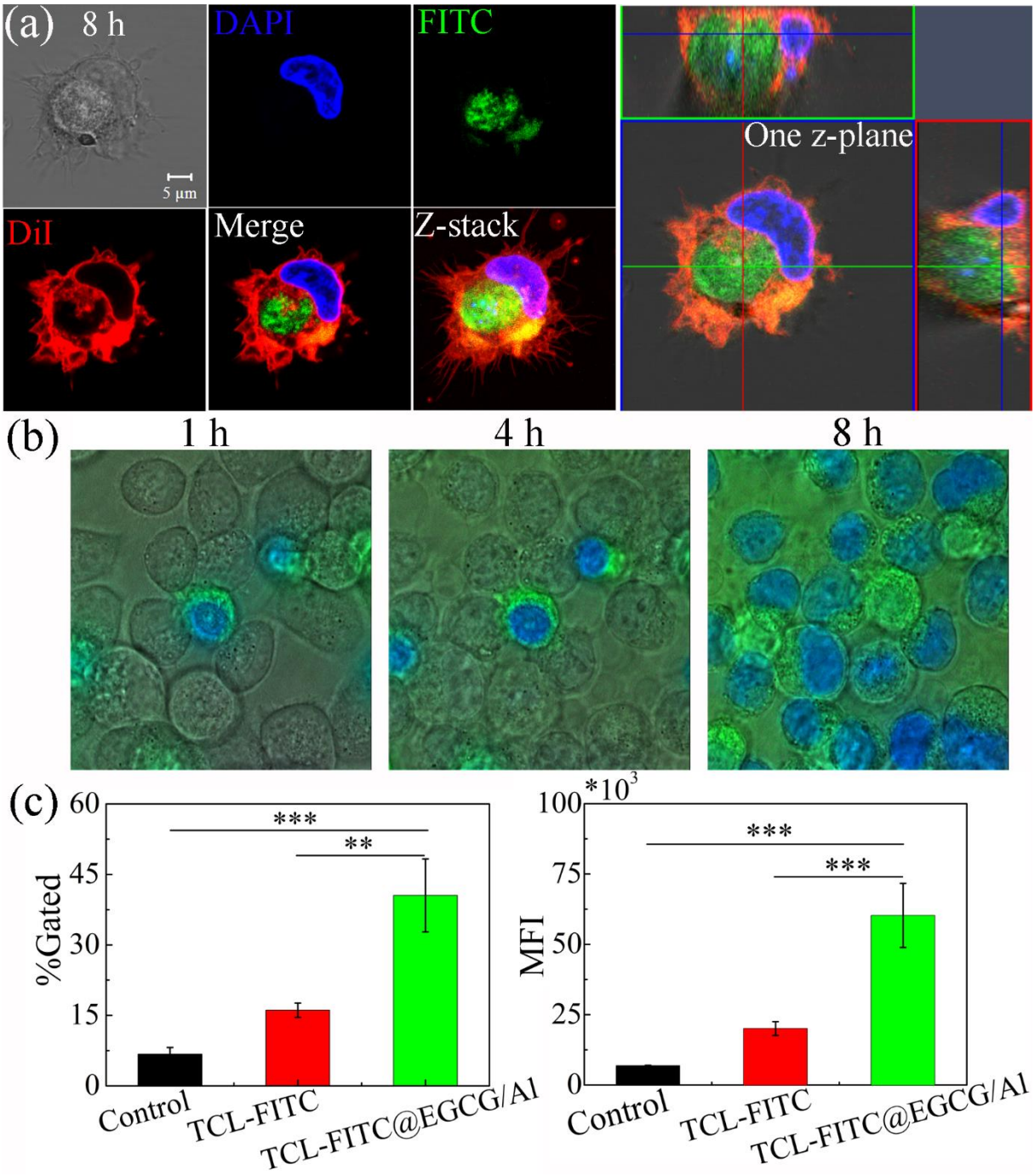

Figure 5. (a) CLSM images of BMDCs pulsed with TCL-FITC@EGCG/Al for 8h, showed the maximum intensity projection of the full z-stack and one z-plane plus corresponding cross sections, (b) Optical images of DC2.4 incubating with TCL@EGCG/Al obtained by live cell imaging systems, (c) DC2.4 cells were incubated with TCL-FITC and TCL-FITC@EGCG/Al for 6 h, the percentage of positive cells (%Gated) and the MFI detected by FACS, the data are

expressed as mean ± SD (n =3), and the differences were analyzed by one way ANOVA with Bonferroni multiple comparison post-test, **p < 0.01, ***p < 0.001.

After antigen uptake, DCs processed and presented antigens to T cells. During the process, DCs were matured and expressed activation markers to prime T cells. BMDCs maturation was characterized by surface marker expression using FACS analysis (**Figure 6a**). Untreated cells served as control. TCL@EGCG/Al induced up-regulation of CD40 and CD80 on BMDCs surface in comparison to the untreated cells and soluble TCL. Furthermore, the expression levels of MHC I and MHC II were also significantly up-regulated, indicating a facilitative role of TCL@EGCG/Al on BMDCs maturation and an enhanced capability to initiate CD8+ and CD4+ T cell priming via MHC I and MHC II pathway, respectively. These observations demonstrated the ability of TCL@EGCG/Al to induce BMDCs maturation and activation, and enhance the antigen presentation ability of BMDCs.

The expression levels of different inflammatory mediators released in the culture medium were also investigated. In comparison with soluble TCL, TCL@EGCG/Al strongly enhanced expression levels of Th1-related cytokines IL-12p70, TNF-α, IL-6 and IFN-γ (Figure 6b), but not of Th2-inducing cytokine IL-4 and IL-10 (**Figure S5**). Specifically, TCL@EGCG/Al caused more than 5-fold increase in the level of cytokines (IL-12p70, TNF-α, and IFN-γ) and 23-fold increase in the level of IL-6 compared to soluble TCL. IL-6 is the recruiting cytokines, play a surprisingly crucial role in APCs recruitment in vivo.[31] Therefore, APCs can be recruited to the vaccine injection site under the regulation of IL-6. TNF-α was a characteristic proinflammatory cytokine with anticancer activity, played a key role in destroying the tumor vascular endothelia. Mature DCs and the IL-12 they produce allow T cells to differentiate into IFN-γ-producing Th1 cells.[32] IFN-γ together with IL-12 promote the differentiation of T cells into CD8+ CTL cells. Therefore, the microparticles triggered the maturation of DCs and the production of Th1-related cytokines revealed their great antitumor potential.

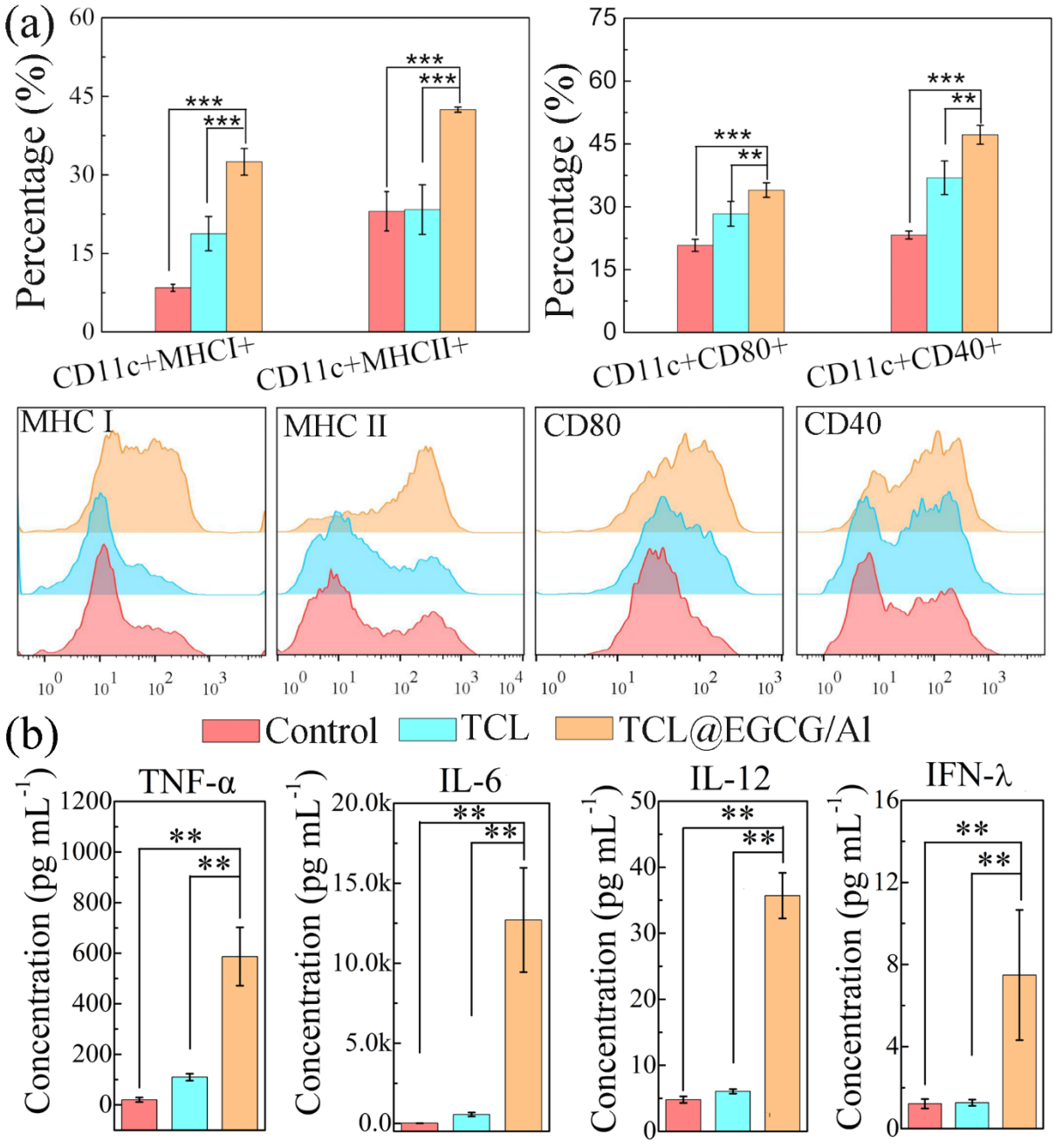

Figure 6. (a) The expression levels of MHCI, MHCII, CD80 and CD40 on $CD11c^+$ BMDCs determined by FACS and their representative FACS histograms, the differences were analyzed using one-way ANOVA with Bonferroni multiple comparison post-test, (b) Secretion of TNF-α, IL-6, IL-12P70 and IFN-γ from BMDCs treated with different formulations, the differences were analyzed using unpaired student's t-test. Data are expressed as mean ± SD (n = 3), **p < 0.01, ***p < 0.001.

2.3. *In vivo* trafficking of TCL@EGCG/Al

Upon antigen uptake and DCs activation, DCs have to reach the lymph nodes, where they will encounter naïve T cells and initiate a specific immune response. The migration process was monitored in real-time *in vivo*. **Figure 7a** shows the representative images of fluorescence signals corresponding to TCL-Cy7 and TCL-Cy7@EGCG/Al at designated time points. The average fluorescence in dLN and injection site were quantified and plotted against time in Figure 7b. After injection for 6 h, Cy7 signal was recorded in dLN for both TCL-Cy7 and TCL-Cy7@EGCG/Al groups, suggesting that the antigen has been migrated to dLN. After injection for 48 h, no signal of Cy7 was recorded in LN for TCL-Cy7 group whereas robust and sustained Cy7 signal was detectable in of TCL-Cy7@EGCG/Al group. This result indicated that the as-prepared microparticles can effectively protect antigens against degradation in vivo and delayed the retention time of antigens in lymph node. After injection, the mean density of Cy7 for TCL-Cy7 retained a constant value in the injection site within 48 h. While the mean density of Cy7 for TCL-Cy7@EGCG/Al was distinctly low after 0 hours of injection due to aggregation-caused quenching (ACQ).[33] After 6 hours of injection, the mean density of Cy7 was increased and afterward retained a constant value, suggesting that TCL-Cy7 have been uptaked by APCs, thus ACQ phen omenon was eliminated.

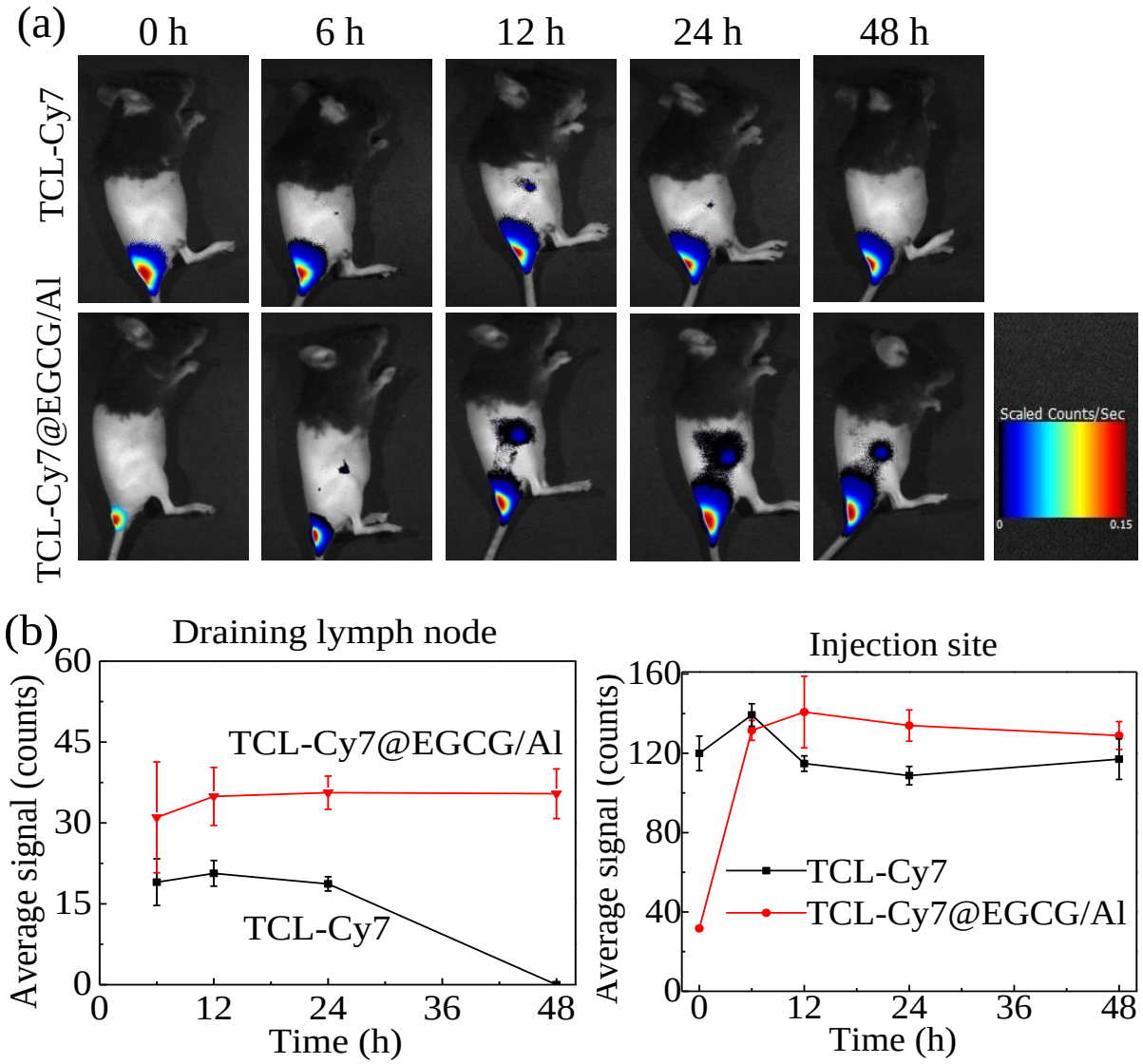

Figure 7. (a) Presence of TCL-Cy7 and TCL-Cy7@EGCG/Al in the injection site and the right draining lymph node, all images were overlays of bright photographs with fluorescence intensity measurement. (b) The mean density of Cy7 in the draining lymph node and the injection site. Data are expressed as mean ± SD (n =3).

2.4. Antitumour immunity of TCL@EGCG/Al in B16 pulmonary metastasis

In order to validate the antitumor efficacy of TCL@EGCG/Al in vivo, B16 pulmonary metastases model was established. PolyI:C (abbreviated as PIC) as TLR-3 agonist has been evaluated as a vaccine adjuvant to enhance the specific antitumor immune responses.[34] Therefore, PIC+free TCL was used as the positive control. On day 4 post inoculation of B16 cells, mice were subcutaneously immunized with various formulations for three times

accordingly. The vaccinations including TCL, TCL+PIC and TCL@EGCG/Al did not cause any obvious side effect on body weight of mice (**Figure 8a**). On day 18 post tumor challenge, photographic images of lungs from immunized mice revealed that TCL@EGCG/Al formulations remarkably decreased the number of tumor nodules in the lung compared to PBS and TCL groups (Figure 8b and **Figure S6**). The result indicated that the vaccination of TCL@EGCG/Al prevented the establishment of pulmonary tumor nodules. Besides, TCL@EGCG/Al exhibited the comparative antitumor effect with TCL+PIC in B16 pulmonary metastasis model. HE staining of lung sections indicated the significant histological changes of the lungs in PBS and TCL groups due to the tumor nodules (Figure 8c). The enlarged photographic images of lung were analyzed by Image J (Figure 8d). And the result illustrated that TCL@EGCG/Al and TCL+PIC showed a similar trend in the expansion of tumor area in lung. Furthermore, TCL@EGCG/Al significantly reduced the expansion of tumor area in lung compared to PBS and TCL groups.

The total serum IgG levels of mice after different treatments were also tested (Figure 8e). There was no statistically significant difference between the four groups with respect to total IgG levels, suggesting that the antitumor effect of TCL@EGCG/Al was not caused by antibody immunity. Furthermore, the cytokine levels (TNF-α, IL-10 and IL-4) of splenocyte culture supernatant after 3 days of antigen restimulation were performed. Splenocyte from TCL@EGCG/Al-treated mice produced greater level of TNF-α, which are associated with enhanced protection than mice treated with other formulations (Figure 8f). Simultaneously, TCL@EGCG/Al did not increase the immunosuppressive cytokine IL-10 (Figure 8g) and the Th2-associated cytokine IL-4 (**Figure S7**), indicating that TCL@EGCG/Al did not increase the proportions of IL-4/IL-10-producing negative regulatory CD4+ T cells. It was all known that negative regulatory CD4+ T cells were detrimental to tumor immunity. In summary, the obtained TCL@EGCG/Al microparticles has superior antitumor effect in B16 pulmonary metastasis in vivo.

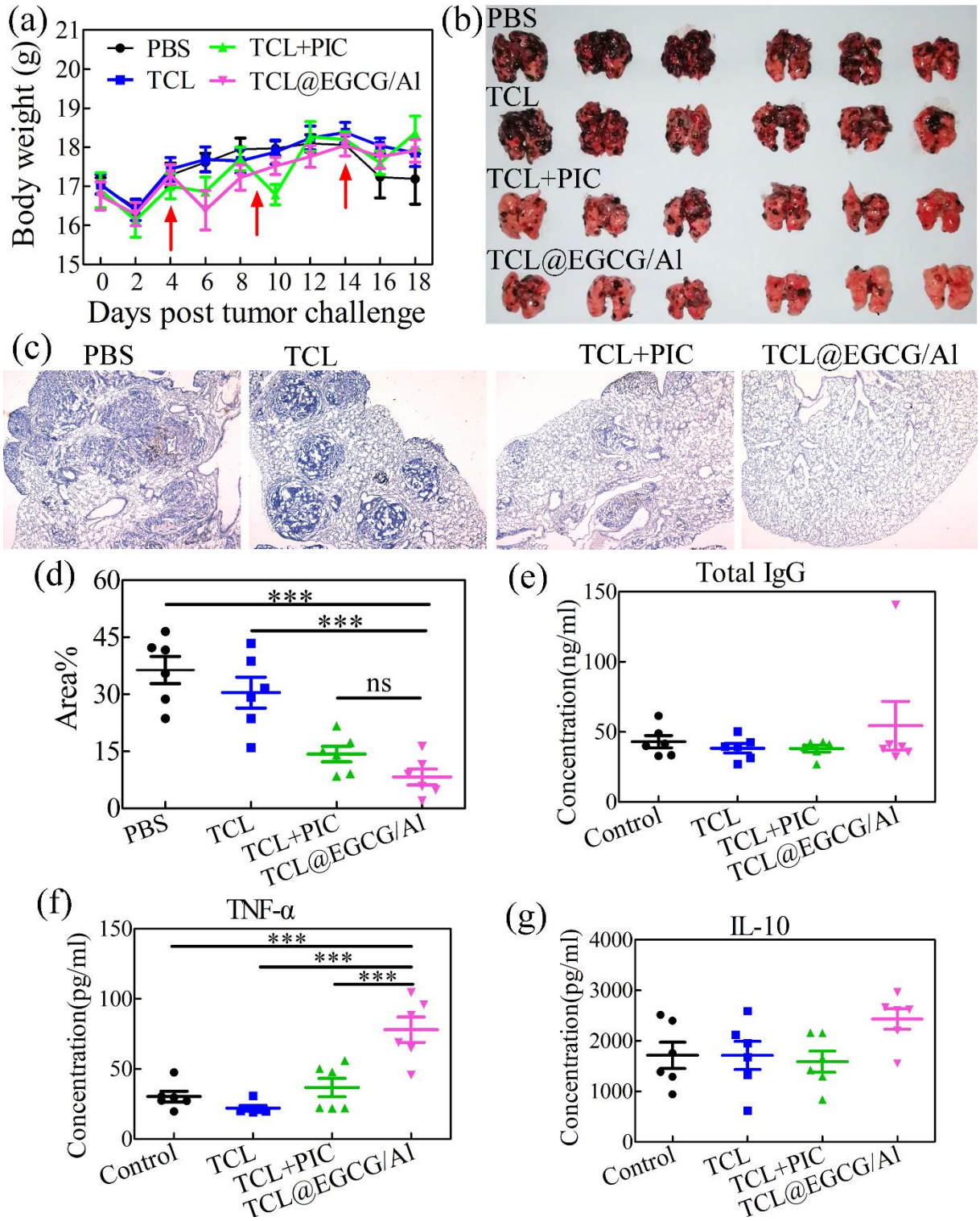

Figure 8. (a) Growth curves of body weight of mice after various treatments, the data are presented as mean ± SEM (n=6), (b) Photographic images of lungs from tumor-bearing mice on day 18 post tumor challenge, (c) Hematoxylin and eosin (HE) staining of mice lung sections after different treatments, the magnifications of all images were 4×, (d) Analysis of the enlarged photographic images of lung in Figure S6 by Image J, and the data were given by the area of

tumor divided by the area of entire lung (Area%), the data are presented as mean ± SEM (n=6) (e) The total serum IgG levels of mice on day 18, (f-g) TNF-α and IL-10 levels of splenocyte culture supernatant after 3 days of antigen stimulation, data are expressed as mean ± SD (n = 6). The differences were analyzed by one way ANOVA with Bonferroni multiple comparison post-test, ***$p < 0.001$.

3. Conclusion

A generic and effective approach to encapsulation of individual cells has been developed by the formation of EGCG/Al coating onto tumor cells. The coating process can be rapidly completed under mild condition, and the materials involved in our strategy are generally regarded as safe by the US Food and Drug Administration. Almost all of the proteins in tumor cell was entrapped within the microparticles, avoiding the antigen loss. Moreover, the coordination bond endowed the microparticles with pH-responsive protein release. More importantly, the microparticles enhanced the uptake efficiency of antigens, protected antigens from degradation in vivo, and delayed the retention time of antigens in lymph node. In addition, the microparticles has the comparative antitumor effect with PolyI:C in pulmonary metastasis model. In principle, this simple and flexible strategy could be extended to other tumor cell types, and provides a novel avenue to personalized cancer immunotherapy.

4. Experimental Section

Materials: 3-[4,5-dimethylthialzol-2-yl]-2,5-diphenyltetrazolium bromide (MTT), aluminium chloride hexahydrate ($AlCl_3 \cdot 6H_2O$) and fluorescein isothiocyanate (FITC) were purchased from Sigma-Aldrich. Epigallocatechin-3-gallate (EGCG, 95%) was purchased from Melone Pharmaceutical Co. Ltd (China). RPMI-1640, DMEM, and fetal bovine serum (FBS) were purchased from Thermofisher (USA). DAPI, red blood cell lysis and cell counting kit-8 (CCK-8) were purchased from Solarbio Science &Technology Co. Ltd (China). Cy7 NHS ester was purchased from ApexBio (USA). BCA Protein Assay Kit and Dil were purchased from Beyotime (China). Poly(I:C) (PIC, HMW VacciGrade™, catalog# vac-pic) were purchased

from InvivoGen (USA). Recombinant mouse GM-CSF and IL-4 were purchased from Peprotech (Rocky, Hill, USA). Anti-mouse monoclonal antibodies (CD80 (B7-1)-FITC, MHCI (H-2Kb)-APC, MHCII (I-Ab)-FITC, CD11c-PerCP-Cy5.5 and CD40-PE) were purchased from eBioscience (USA). Mouse Total IgG ELISA Kit was purchased from neobioscience (China). Mouse cytokines ELISA kit (IL-10, TNF-α, IL-4) were purchased form ebioscience (USA). All chemicals were used without further purification.

Cell lines and animals: The immortalized mouse dendritic cells line DC2.4, murine melanoma cells line B16 and human acute myeloid leukemia cells line HL-60 were purchased from the Cell Bank of China Academy of Sciences, and cultured according to the manufacture's guidelines. Mouse urothelial carcinoma cells line MB49, colon carcinoma cell line CT26, breast cancer cell line 4T1 were purchased from China Infrastructure of Cell Line Resource. Female C57BL/6 (6-8 weeks old) mice were purchased from Vital River Laboratory Animal Technology Co., Ltd. (China), and raised under SPF conditions. All animals operation was in compliance with the regulations of the Tianjin Committee of Use and Care of Laboratory Animals, and the overall project protocol was approved by the Animal Ethics Committee of the Chinese Academy of Medical Science.

Encapsulation of tumor cells and preparation of TCL@EGCG/Al: B16 cells were detached and single cell suspension was obtained (2×10^6 cells/mL). Then, EGCG (0.5 mL, 20 mg mL^{-1}) and $AlCl_3$ (0.5 mL, 5 mg mL^{-1}) aqueous solutions were added to 9 mL of the cell suspension. The cell suspension was vigorously mixed for 60 s immediately after the additions of EGCG and $AlCl_3$. Then the cells were centrifuged (200 g, 3 min) and washed with isotonic saline solution to remove excess EGCG and $AlCl_3$ after each layer deposition. This coating process was repeated three times, B16@EGCG/Al were prepared. After coating, the cells were incubated in high-purity water for 30 min to kill the cells, and tumor cell lysates (TCL)-containing microparticles (TCL@EGCG/Al) were obtained. The whole process was performed at 4 ^oC to block energy-dependent internalization pathways. The loading capacity represented the ratio of

protein amount encapsulated in the microparticles to the microparticles weight. SEM and TEM images of TCL@EGCG/Al were performed. As a control, TCL was obtained by five repeated freeze-thaw cycles as previously reported in the literature, and diluted to required concentration before use.[35]

4T1, CT26, MB49 and HL-60 cells were also encapsulated by EGCG/Al layer, then CLSM images and SEM images of these cells before and after coating were conducted. Uncoated cells were co-cultured with FITC-containing DMSO and medium mixture at 37 °C for 30 min, then the FITC-labelled cells were washed twice with PBS. CLSM images of uncoated cells were conducted after fixation of FITC-labelled cells with paraformaldehyde followed by labeled with DAPI. CLSM images of the coated cells were also conducted after the coating of FITC-labelled cells followed by labeled with DAPI. TEM images of uncoated cells were fixed by glutaraldehyde followed by washing with high-purity water.

Proteins release from TCL@EGCG/Al: The amount of proteins released from TCL@EGCG/Al were measured under pH 5.5 and pH 7.4. TCL@EGCG/Al containing 4 mg of TCL were suspended in 4 mL of PBS and incubated at 37 ^{o}C with continuous agitation in an orbital shaker. The suspension was centrifuged at 3000 rpm for 5 min at designated time points. 2 mL of supernatants were collected and stored at -80 ^{o}C for analysis. Then 2 mL of fresh PBS was added to the original tube. Proteins in supernatants were tested using BCA assay. The cumulative release of protein was presented as a function of time.

Stability of TCL@EGCG/Al: The stability of TCL@EGCG/Al was evaluated by suspending the microparticles vaccine in culture medium containing a known concentration of BSA or FBS and incubated at 37 ^{o}C. At regular intervals, the microparticles suspension was centrifuged and the concentration of BSA or FBS in the supernatant was measured by BCA. Then, the concentration of BSA or FBS was given as a function of time. Besides, optical images were

taken after suspending the microparticles in culture medium containing BSA or FBS for a period of time.

Generation of BMDCs and antigens uptake: C57BL/6 mice were sacrificed and bone marrow was flushed out of femur and tibia. After red blood cell lysis, cells were seeded in six-well plates (2×10^5 cells/ml) and incubated at 37 °C in 5% CO_2. Culture medium was RPMI-1640 supplemented with 10% FBS, 1% penicillin/streptomycin, 10 ng/ml IL-4 and 20 ng/ml GM-CSF. On day 6 of culture, the non-adherent cells were harvested and immature BMDC cells were obtained. B16 cells were labeled with FITC according to the reported method,[25, 36] then, TCL-FITC and TCL-FITC@EGCG/Al were obtained with FITC-labeled B16 cells according to the preparation process of TCL and TCL@EGCG/Al. And the fluorescent spectra of TCL-FITC and TCL-FITC@EGCG/Al were presented in **Figure S1**. Immature BMDCs (5×10^5 cells/mL) were cultured with TCL-FITC@EGCG/Al for 8 h. After the incubation, the cells were washed twice with PBS, stained with DAPI and Dil. The fluorescent images were recorded by CLSM (CarlZeiss LSM710). DC2.4 cells were seeded in 24-well plate (1×10^6 cells/well) and incubated with TCL-FITC and TCL-FITC@EGCG/Al for 6 h, the dosage of TCL-FITC was 20 ug/well. After extensive washing, the antigen uptake was determined by FACS analysis.

Stimulation and activation of BMDCs: Immature BMDCs were plated in 24-well plates (5×10^5 cells/ml). Then, TCL and TCL@EGCG/Al were added to make final TCL concentration of 10 μg/ml. After 48 h of culture, cells were centrifuged and analyzed by FACS analysis (BD Pharmingen) after staining with CD11c in combination with CD40 and CD80 or MHCI and MHCII. And the supernatant was collected and stored at -80 °C for cytokines determination by using a mouse Magnetic Luminex Screening assay for IL-12p70, TNF-α, IFN-γ, IL-6, IL-4 and IL-10 according to the manufacturer's protocol (R&D Systems) on a Luminex 200. Untreated cells and cells incubated with LPS served as negative and positive controls, respectively.

In vivo trafficking of TCL@EGCG/Al: To prepare TCL-Cy7 and TCL-Cy7@EGCG/Al, B16 cells were first labeled with Cy7 according to the labeling method of FITC. Then, TCL-Cy7

and TCL-Cy7@EGCG/Al were obtained with Cy7-labeled B16 according to the preparation process of TCL and TCL@EGCG/Al as described above. And the fluorescent spectra of TCL-Cy7 and TCL-Cy7@EGCG/Al were presented in **Figure S2**. Female C57BL/6 mice were injected subcutaneously at the tail base with TCL-Cy7 and TCL-Cy7@EGCG/Al containing 150 μg of TCL-Cy7 dispersed in 100 μl PBS. Then mice were visualized at the injection site and the adjacent lymph node (LN), where immune responses were initiated.[37] Vaccine kinetics was then studied at several time points after administration by *in vivo* imaging system (Maestro, CRI USA). Mice were anesthetized by inhalation of isoflurane and fluorescence spectral cubes were acquired using near infrared preset filter. Unmixed images in which background signals were subtracted and quantified by using Maestro software.

Antitumor therapeutic of TCL@EGCG/Al in B16 pulmonary metastasis model: Female 6-8 weeks C57BL/6 mice were i.v. injected via tail vein with 1×10^5 B16 cells suspended in 100 μL PBS at day 0, and randomly assigned into four groups (n=6): 1) Control, 2) TCL, 3) TCL+PIC, and 4) TCL@EGCG/Al. Mice were monitored every other day for body weight. On day 4, 9 and 14, mice were s.c. immunized with 100 μL the corresponding samples containing 200 ug of TCL. Mice were sacrificed at day 18 by cervical dislocation, and the spleen and lung were isolated for further analysis. Venous blood of mice was collected and serum was isolated. Serum total IgG level was measured using Mouse Total IgG ELISA kit. Lungs were fixed in 4% formalin, embedded in paraffin, sectioned and stained with hematoxylin and eosin (HE). Single cells suspension of spleen was prepared and plated in 96-well plate (5×10^6 cells/ml), restimulated with 40 ug mL^{-1} of TCL for 72 h, then the culture supernatant was collected for determining cytokine concentrations by ELISA assay.

Statistical Analysis: All results except that in Figure 8a,d, which are presented as the mean ± standard error of the mean (SEM), are presented as the mean ± standard deviation (SD), as indicated. Statistical analysis for all tests except that in Figure 6b, which is carried out using uppaired Student's t-test, is carried out using one way ANOVA with Bonferroni's Multiple

Comparison Test. Sample size (n) for all statistical analysis except that in Figure 4c-e and Figure 8 (n=6) is 3. All statistics were performed in GraphPad Prism (PRISM7.0; GraphPad Software). The threshold for statistical significance was $P<0.05$.

Supporting Information

Supporting Information S1 and Supporting Information Video S2 are available from the Wiley Online Library or from the author.

Acknowledgements

The authors thank for the National Natural Science Foundation of China (31600743, 81673027, 31771097), Specific Program for High-Tech Leader&Team of Tianjin Government, Natural Science Foundation of Tianjin City (17JCZDJC37400, 18JCQNJC14500), CAMS Innovation Fund for Medical Sciences (CAMS-I2M-3-026), Tianjin Natural Science Fund for Distinguished Young Scholars (17JCJQJC46400), PUMC Youth Fund & the Fundamental Research Funds for the Central Universities (2017310031).

Received: ((will be filled in by the editorial staff))
Revised: ((will be filled in by the editorial staff))
Published online: ((will be filled in by the editorial staff))

References

[1] I. Mellman, G. Coukos, G. Dranoff, *Nature* **2011**, *480*, 480.
[2] K. Kakimi, T. Karasaki, H. Matsushita, T. Sugie, *Breast Cancer* **2017**, *24*, 16.
[3] a) M. F. Bachmann, G. T. Jennings, *Nat. Rev. Immunol.* **2010**, *10*, 787; b) V. K. Sondak, J. A. Sosman, *Semin. Cancer Biol.* **2003**, *13*, 409.
[4] S. Srivatsan, J. M. Patel, E. N. Bozeman, I. E. Imasuen, S. He, D. Daniels, P. Selvaraj, *Hum. Vaccines Immunother.* **2013**, *10*, 52.
[5] a) C. L. Chiang, L. E. Kandalaft, G. Coukos, *Int. Rev. Immunol.* **2011**, *30*, 150; b) L. L. Chiang, G. Coukos, L. E. Kandalaft, *Vaccines* **2015**, *3*, 344.
[6] a) E. J. Small, N. Sacks, J. Nemunaitis, W. J. Urba, E. Dula, A. S. Centeno, W. G. Nelson, D. Ando, C. Howard, F. Borellini, *Clin. Cancer Res.* **2007**, *13*, 3883; b) H. Wu, Y. Han, Y. Qin, C. Cao, Y. Xia, C. Liu, Y. Wang, *Oncol. Rep.* **2013**, *29*, 529.
[7] R. L. Coffman, A. Sher, R. A. Seder, *Immunity* **2010**, *33*, 492.
[8] a) L. Vandenberk, J. Belmans, M. Van Woensel, M. Riva, S. W. Van Gool, *Front. Immunol.* **2016**, *6*, 663; b) S. Anguille, E. L. Smits, E. Lion, V. F. van Tendeloo, Z. N. Berneman, *Lancet Oncol.* **2014**, *15*, e257.
[9] L. Lybaert, K. A. Ryu, L. Nuhn, R. D. Rycke, O. D. Wever, A. C. Chon, A. P. EsserKahn, B. G. D. Geest, *Chem. Mater.* **2017**, *29*, 4209.
[10] G. N. Shi, C. N. Zhang, R. Xu, J. F. Niu, H. J. Song, X. Y. Zhang, W. W. Wang, Y. M. Wang, C. Li, X. Q. Wei, *Biomaterials* **2017**, *113*, 191.
[11] M. O. Hardin, T. J. Vreeland, G. T. Clifton, D. F. Hale, G. S. Herbert, J. M. Greene, D. O. Jackson, J. E. Berry, P. Nichols, S. Yin, *Immunotherapy* **2018**, *10*, 373.
[12] B. P. Gross, A. Wongrakpanich, M. B. Francis, A. K. Salem, L. A. Norian, *AAPS J.* **2014**, *16*, 1194.
[13] Y. W. Noh, S. Y. Kim, J. E. Kim, S. Kim, J. Ryu, I. Kim, E. Lee, S. H. Um, T. L. Yong, *Adv. Funct. Mater.* **2017**, *27*, 1605398.
[14] a) R. H. Fang, C.-M. J. Hu, B. T. Luk, W. Gao, J. A. Copp, Y. Tai, D. E. O'Connor, L. Zhang, *Nano Lett.* **2014**, *14*, 2181; b) A. V. Kroll, R. H. Fang, Y. Jiang, J. Zhou, X. Wei, C. L. Yu, J. Gao, B. T. Luk, D. Dehaini, W. Gao, *Adv. Mater.* **2017**, *29*, 1018.

[15] S. A. Bencherif, R. Warren Sands, O. A. Ali, W. A. Li, S. A. Lewin, T. M. Braschler, T.-Y. Shih, C. S. Verbeke, D. Bhatta, G. Dranoff, D. J. Mooney, *Nat. Commun.* **2015**, *6*, 7556.

[16] X. Huang, D. Ye, P. E. Thorpe, *Vaccine* **2011**, *29*, 4785.

[17] L. Chakrabarti, C. Morgan, A. D. Sandler, *Plos One* **2015**, *10*, e0129237.

[18] L. Lybaert, E. De Vlieghere, R. De Rycke, N. Vanparijs, O. De Wever, S. De Koker, B. G. De Geest, *Adv. Funct. Mater.* **2014**, *24*, 7139.

[19] a) I. Haubera, H. Hohenberg, B. Holstermann, W. Hunstein, J. Hauber, *Proc. Natl. Acad. Sci. U. S. A.* **2009**, *106*, 9033; b) J. E. Chung, S. Tan, S. J. Gao, N. Yongvongsoontorn, S. H. Kim, J. H. Lee, H. S. Choi, H. Yano, L. Zhuo, M. Kurisawa, J. Y. Ying, *Nat. Nanotechnol.* **2014**, *9*, 907.

[20] K. Matsunaga, T. W. Klein, H. Friedman, Y. Yamamoto, *Infect. Immun.* **2001**, *69*, 3947.

[21] a) Y. I. Jeong, I. D. Jung, J. S. Lee, C. M. Lee, J. D. Lee, Y. M. Park, *Biochem. Biophys. Res. Commun.* **2007**, *354*, 1004; b) K. Ogawa, T. Hara, M. Shimizu, S. Ninomiya, J. Nagano, H. Sakai, M. Hoshi, H. Ito, H. Tsurumi, K. Saito, *Cancer Sci.* **2012**, *103*, 951.

[22] a) M. Kumamoto, T. Sonda, K. Nagayama, M. Tabata, *Biosci. Biotech. Bioch.* **2001**, *65*, 126; b) M. B. Inoue, M. Inoue, Q. Fernando, S. Valcic, B. N. Timmermann, *J. Inorg. Biochem.* **2002**, *88*, 7.

[23] a) H. Ejima, J. J. Richardson, K. Liang, J. P. Best, M. P. van Koeverden, G. K. Such, J. Cui, F. Caruso, *Science* **2013**, *341*, 154; b) M. A. Rahim, K. Kempe, M. Müllner, H. Ejima, Y. Ju, M. P. van Koeverden, T. Suma, J. A. Braunger, M. G. Leeming, B. F. Abrahams, F. Caruso, *Chem. Mater.* **2015**, *27*, 5825.

[24] J. H. Park, K. Kim, J. Lee, J. Y. Choi, D. Hong, S. H. Yang, F. Caruso, Y. Lee, I. S. Choi, *Angew. Chem. Int. Ed.* **2014**, *53*, 12420.

[25] X. Wang, J. Liang, C. Zhang, G. Ma, C. Wang, D. Kong, *Chem. Commun.* **2019**, *55*, 1568.

[26] Q. Liu, X. Chen, J. Jia, W. Zhang, T. Yang, L. Wang, G. Ma, *ACS Nano* **2015**, *9*, 4925.

[27] P. Zhang, Y. C. Chiu, L. H. Tostanoski, C. M. Jewell, *ACS Nano* **2015**, *9*, 6465.

[28] K. T. Mody, A. Popat, D. Mahony, A. S. Cavallaro, C. Yu, N. Mitter, *Nanoscale* **2013**, *5*, 5167.

[29] Y. Ping, J. Guo, H. Ejima, X. Chen, J. J. Richardson, H. Sun, F. Caruso, *Small* **2015**, *11*, 2032.

[30] T. Okuda, T. Yoshida, T. Hatano, *Basic Life Sci.* **1992**, *59*, 539.

[31] G. Kaplanski, V. Marin, F. Montero-Julian, A. Mantovani, C. Farnarier, *Trends Immunol.* **2003**, *24*, 25.

[32] a) F. Koch, U. Stanzl, P. Jennewein, K. Janke, C. Heufler, E. Kämpgen, N. Romani, G. Schuler, *J. Exp. Med.* **1996**, *184*, 741; b) C. Reis e Sousa, S. Hieny, T. Scharton-Kersten, D. Jankovic, H. Charest, R. N. Germain, A. Sher, *J. Exp. Med.* **1997**, *186*, 1819.

[33] a) X. Ma, R. Sun, J. Cheng, J. Liu, F. Gou, H. Xiang, X. Zhou, *J. Chem. Educ.* **2016**, *93*, 345; b) J. Wu, W. Liu, J. Ge, H. Zhang, P. Wang, *Chem. Soc. Rev.* **2011**, *40*, 3483.

[34] F. Steinhagen, T. Kinjo, C. Bode, D. M. Klinman, *Vaccine* **2011**, *29*, 3341.

[35] L. Alaniz, M. M. Rizzo, G. Mazzolini, *Pulsing Dendritic Cells with Whole Tumor Cell Lysates*, Springer New York, **2014**.

[36] E. C. Butcher, I. L. Weissman, *J. Immunol. Methods* **1980**, *37*, 97.

[37] M. Sixt, N. Kanazawa, M. Selg, T. Samson, G. Roos, D. P. Reinhardt, R. Pabst, M. B. Lutz, L. Sorokin, *Immunity* **2005**, *22*, 19.

Supporting Information

A generic coordination assembly-enabled nanocoating of individual tumor cells for personalized immunotherapy

Xiaoli Wang,‡[a] Zuoguan Chen,‡[b] Chao Zhang,[a] Chuangnian Zhang,[a] Guilei Ma,[a] Jing Yang,[a] Xiaoqing Wei,*[c] Hongfan Sun[a]*

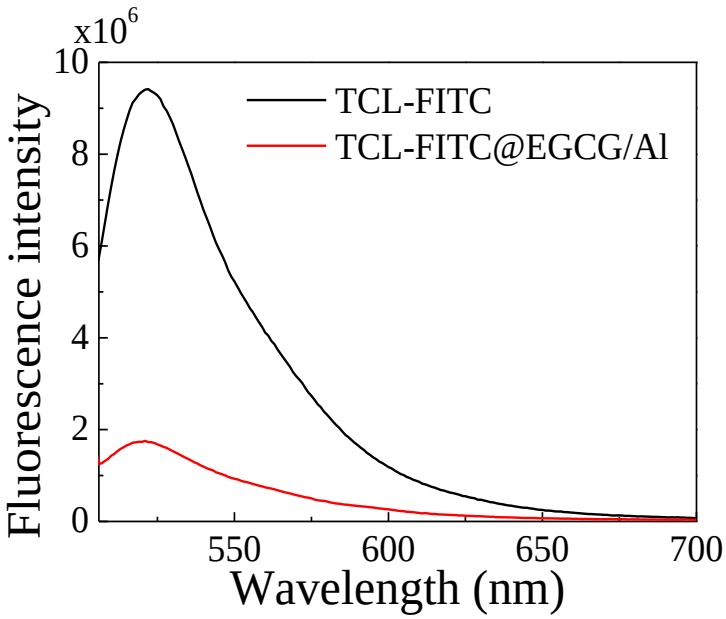

Figure S1. The fluorescence spectra of TCL-FITC and TCL-FITC@EGCG/Al in water, the excitation wavelength was 495 nm, the concentration of TCL-FITC in all the formulations was 10 μg ml^{-1}. The fluorescence intensity of TCL-FITC was obviously higher than that of TCL-FITC@EGCG/Al although the concentration of TCL-FITC in all the formulations was the same. This phenomenon was notoriously known as fluorescence aggregation-caused quenching (ACQ).[1, 2] Because of the high protein loading capacities, the concentration of TCL-FITC within microparticles were quite high, thus the aggregation of TCL-FITC caused fluorescence quenching.

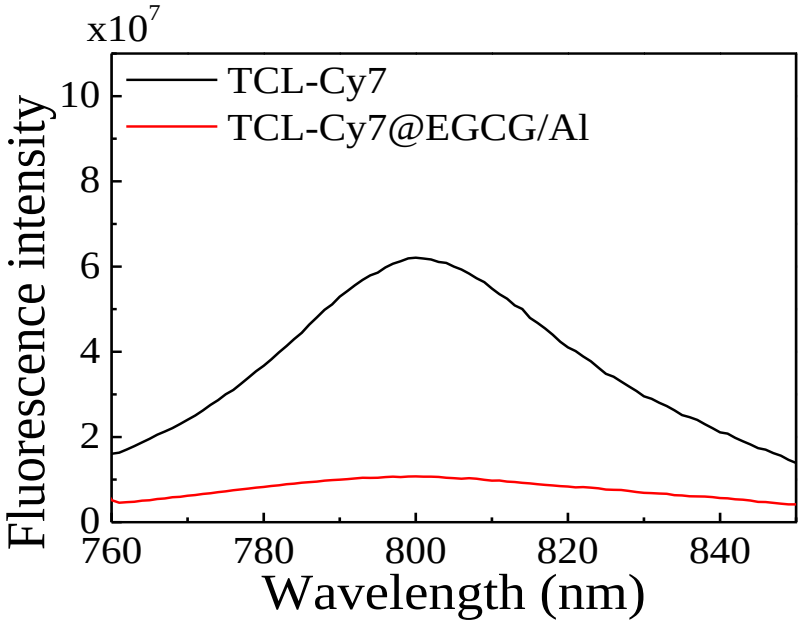

Figure S2. The fluorescence spectra of TCL-Cy7 and TCL-Cy7@EGCG/Al in water, the excitation wavelength was 750 nm, the concentration of TCL-Cy7 in all the formulations was 0.3 mg ml^{-1}.

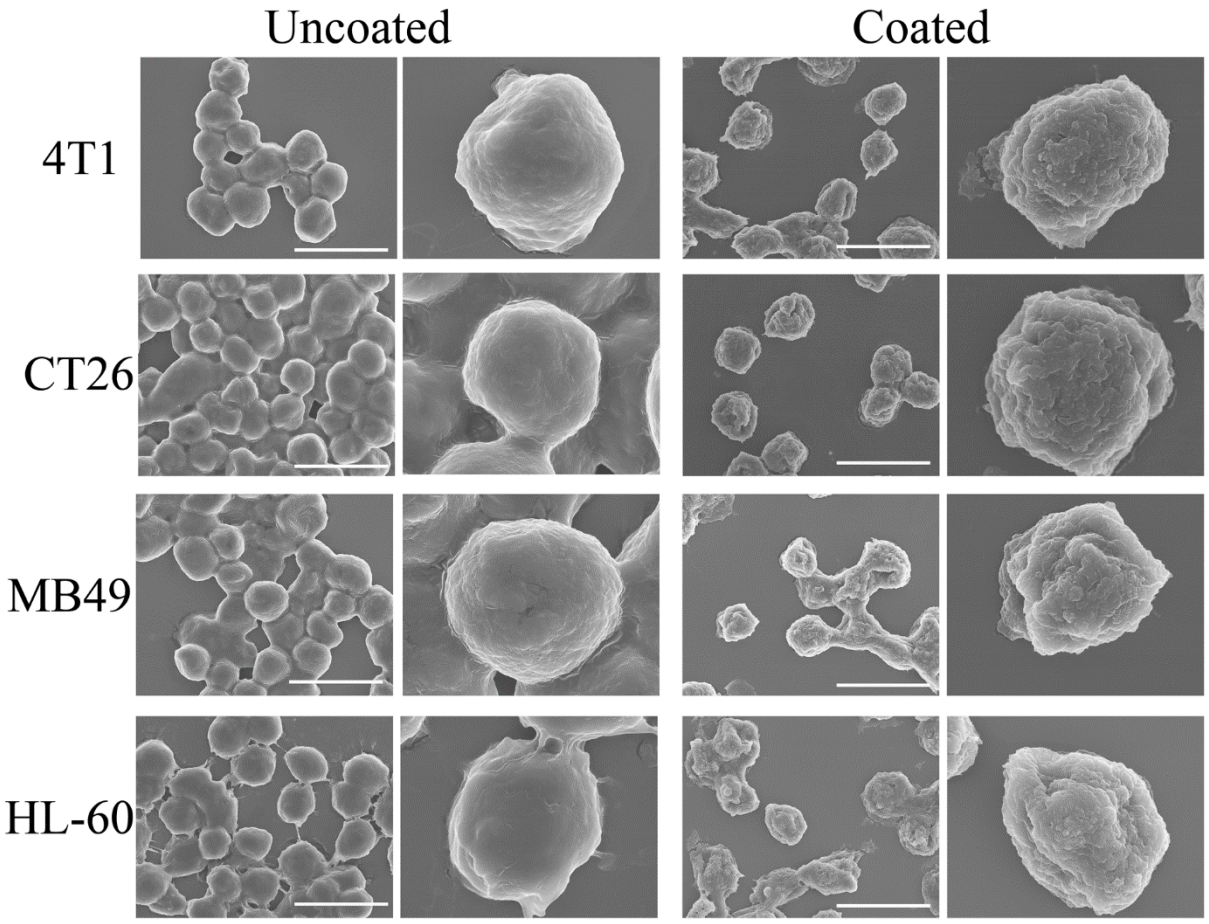

Figure S3. SEM images of 4T1, CT26, MB49 and HL-60 cells before and after coating by EGCG/Al layer. Uncoated cells were fixed by glutaraldehyde followed by washing with high-purity water. The ruler was 20 μm.

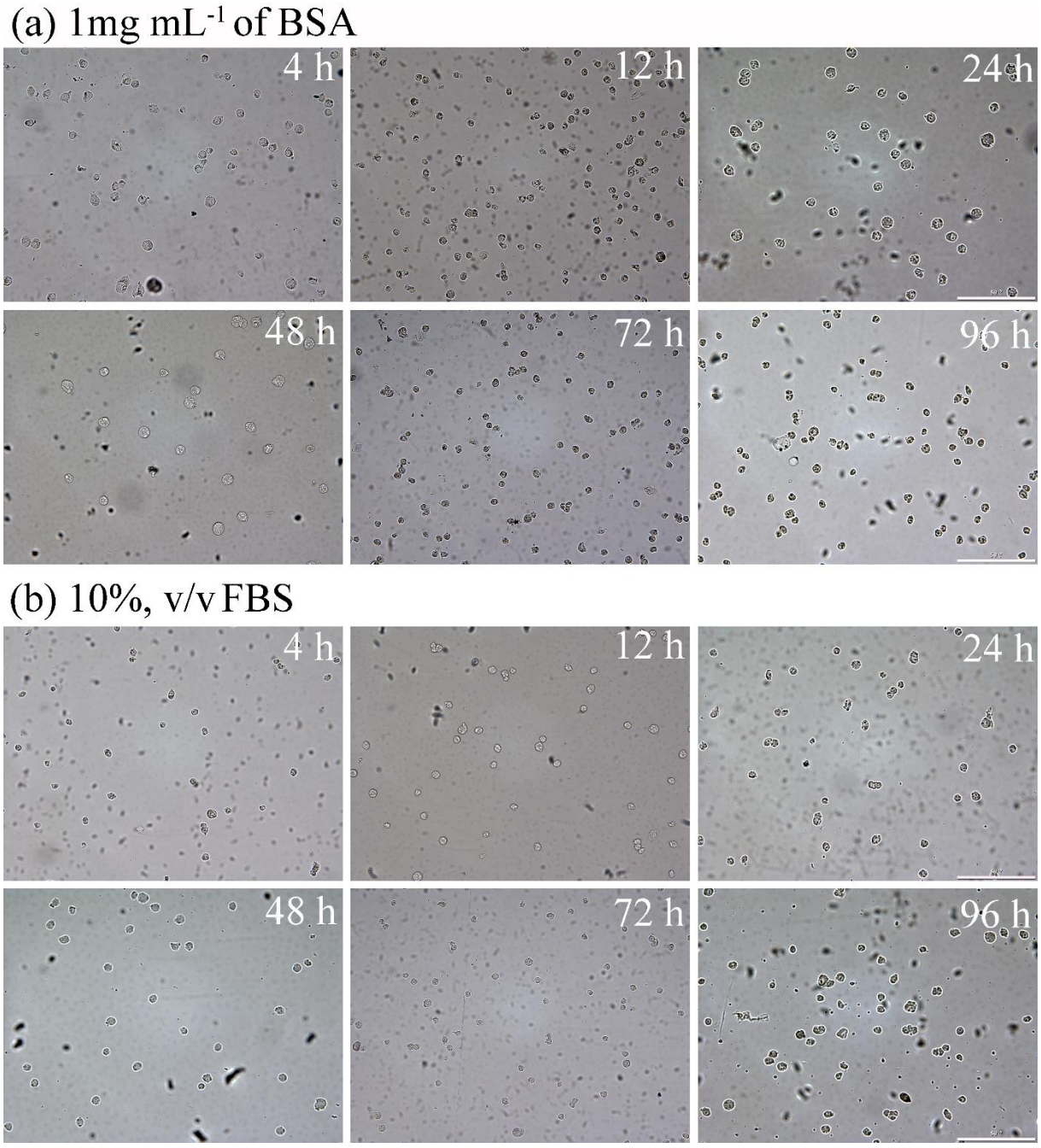

Figure S4. The optical images of TCL@EGCG/Al after suspending the microparticles vaccine in culture medium containing a known concentration of BSA or FBS at 37 ºC for a period of time.

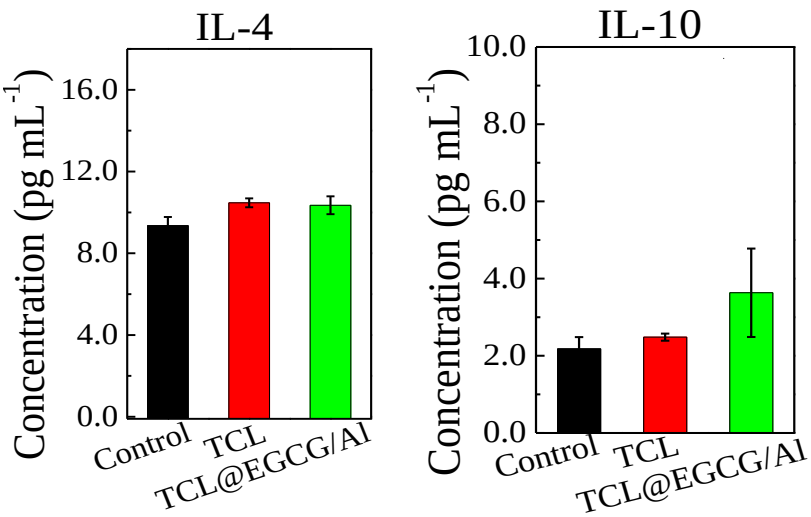

Figure S5. Secretion of IL-4 and IL-10 from BMDCs treated with different formulations, the differences were analyzed using unpaired student's t-test. *p < 0.05, **p < 0.01, ***p < 0.001.

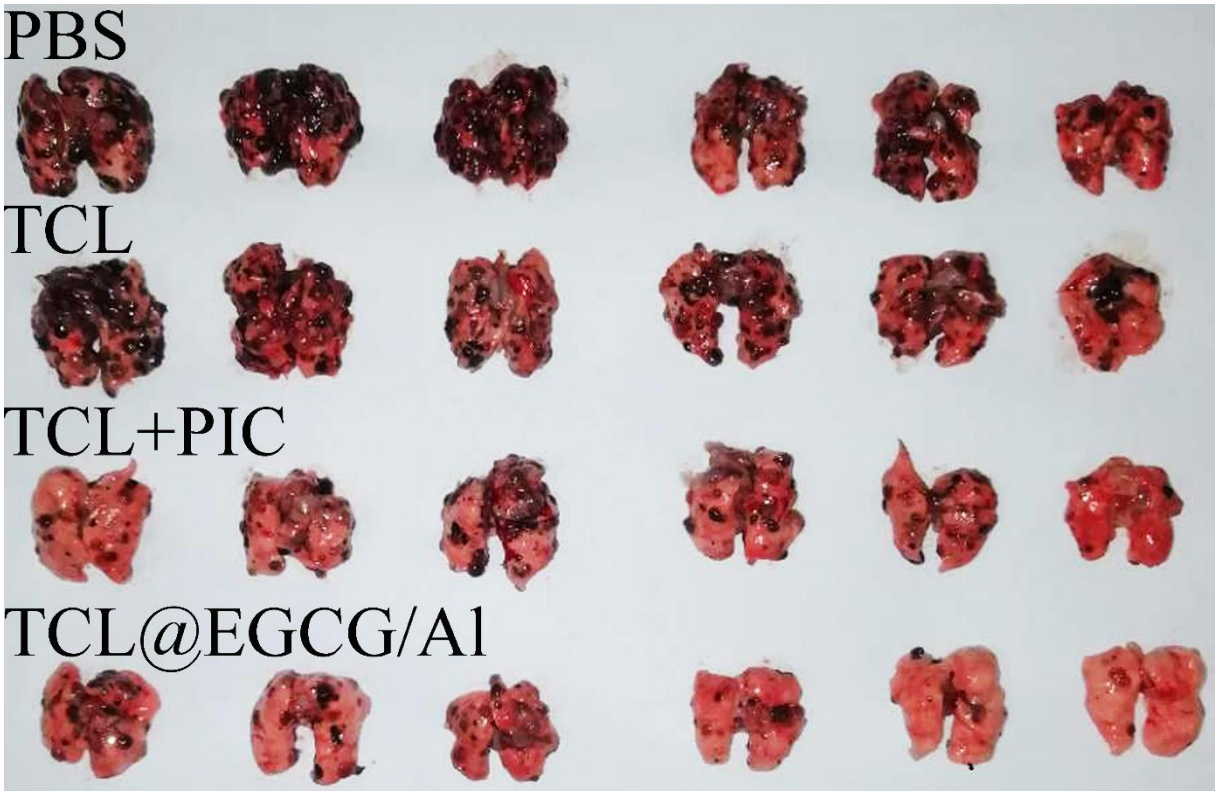

Figure. S6 Photographic images of lungs from tumor-bearing mice on day 18 post tumor challenge

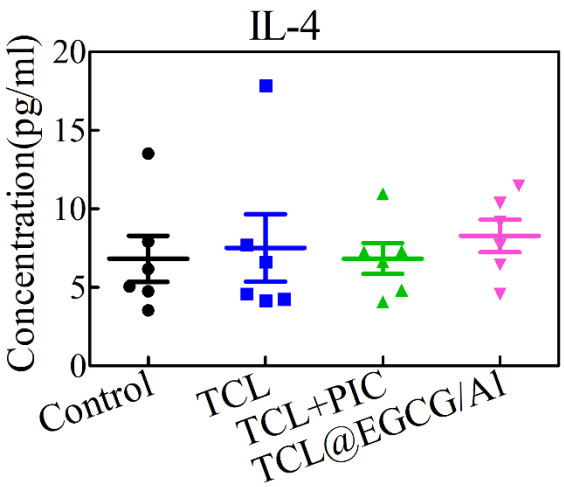

Figure. S7 IL-4 level of splenocyte culture supernatant after 3 days of antigen stimulation, the data are expressed as mean ± SD (n = 6), the differences were analyzed by one way ANOVA with Bonferroni multiple comparison post-test.

References

[1] a) X. Ma, R. Sun, J. Cheng, J. Liu, F. Gou, H. Xiang, X. Zhou, *J. Chem. Educ.* **2016**, 93, 345; b) J. Wu, W. Liu, J. Ge, H. Zhang, P. Wang, *Chem. Soc. Rev.* **2011**, 40, 3483.